Wave Propagation Mechanisms for Intra-Chip Communications

Liping Yan, *Member, IEEE*, and George W. Hanson, *Fellow, IEEE*

***Abstract*—Fundamental wave propagation mechanisms for intra-chip communications in a multilayered IC chip structure are studied theoretically and numerically. The well-known Green's function representation in terms of branch cuts (continuous spectrum), residues (discrete spectrum), and direct source-receiver radiation is used to clarify important wave processes for typical intra-chip antenna structures. It is found that surface waves may or may not provide the dominant propagation channel contribution, depending on frequency and chip structure. We generalize the concept of multipath to include multiple spectral (e.g., discrete and continuous) wave components, appropriate for the near- and intermediate-field problems of interest for chip-scale propagation. The effect of a guiding layer placed either below or above the silicon substrate is considered. It is found that a guiding layer can provide enhanced single-channel signal transmission via the surface wave channel, and thereby reduce dispersion associated with multi wave component effects.**

***Index Terms*—Electromagnetic surface wave, Green function, multilayered media.**

I. Introduction

In order to improve device performance, the continuous downscaling of dimensions in CMOS technology leads to great challenges for traditional metal line interconnects [1]. To solve this problem, wireless interconnects and chip-area networks have been proposed for the development of ultra-large scale integration (ULSI) or system-on-chip (SoC) architectures. Recent research has focused on device designs and integrated antennas for wireless interconnect applications [2]–[12]. However, aside from previous work in [9], [12], the basic propagation mechanisms on integrated chip structures have not been carefully studied, despite their importance for the development of intra-chip wireless communications.

In 1998, Kim and K. O studied the characteristics of integrated dipole antennas on bulk, silicon-on-insulator (SOI) and silicon-on-sapphire (SOS) substrates for wireless communication [8]. Measurements confirm signal transmission, and show that the gain of an antenna pair on an SOS substrate is higher than that on bulk and SOI substrates due to conduction loss and reflections from substrates. Later, Kim *et al.* proposed a plane wave model to understand the propagation in an intra-chip communication system [9]. They measured the gain from 6 to 18 GHz using two integrated dipole antennas separated by 5 mm and mounted on a silicon wafer, with or without a bottom dielectric layer. Results showed that the transmission gain can be improved by inserting a low-loss dielectric layer between the silicon wafer and ground plane. Guo *et al.* found from measurements that inserting an aluminum nitride (AlN) layer, which acts as a propagation medium, between a silicon wafer containing integrated antennas and the ground plane improves the antenna transmission gain by 8 dB at 15 GHz [10] (we support this finding here). Kikkawa *et al.* studied the effect of silicon substrates on the transmission characteristics of integrated antennas, and found that the transmission gain can be improved by increasing silicon resistivity [11]. Zhang and Chen have investigated the propagation mechanism of radio waves over intra-chip channels by measuring the S-parameters from 10 to 110 GHz, and by considering path loss and delay spread [12]. They found that the path loss exponent (PLE) of the intra-chip channel is significantly lower than the free-space PLE, and that the time of first signal arrival is significantly later than would be the case for free-space propagation. Consequently, they concluded that the dominant contribution to the received signal is through a surface wave, rather than via space waves.

In general, there are several wave components that lead to different propagation paths (both physical and spectral) in a multilayer chip structure: a discrete spectrum, consisting of surface waves guided by the layered medium [13]–[15], [16], a continuous spectrum, representing radiation modes of the layered medium [14]–[17] (which contain both propagating and non-propagating spectra—radiative and reactive effects, respectively), and, when a line-of-sight exists between source and receiver, a direct space-wave radiation component. Each wave component travels with different propagation characteristics (phase/group velocity, attenuation), such that dispersion/distortion and interference can become important issues.

In order to have a better understanding of the contributions from different wave components to the total electric field, in this work we use the Green function for a layered medium, evaluated via complex-plane analysis, to separate the discrete and continuous spectral field components. This model, containing both physically different propagation paths (direct radiation and guided energy), and multispectral components (discrete and continuous spectra), can be considered to be a generalization of the usual ray-based idea of multipath.

The complex-plane analysis of the Green's function for layered media is well-known [13]–[15], and has been used extensively in the past to both interpret propagation physics, and to

Manuscript received December 01, 2008; revised April 05, 2009. First published July 10, 2009; current version published September 02, 2009.

L. Yan is with the College of Electronics and Information Engineering, Sichuan University, Chengdu 610064, China (e-mail: sherryyan05@gmail.com).

G. W. Hanson is with the Department of Electrical Engineering, University of Wisconsin-Milwaukee, Milwaukee, WI 53211 USA (e-mail: george@uwm.edu).

Color versions of one or more of the figures in this paper are available online at http://ieeexplore.ieee.org.

Digital Object Identifier 10.1109/TAP.2009.2027158

obtain efficient methods for evaluating Sommerfeld integrals. For example, in [18]–[24] representations of layered-medium Green's functions have been obtained in terms of combinations of quasi-static and quasi-dynamic images, discrete complex images, surface waves, leaky waves, and various steepest-descent representations. All of these methods lead to both numerical efficiency (although with varying levels of ease in evaluation and generality) and physical insight, and may be of use to the intra-chip propagation problem studied here. In this paper we use the residues-plus-branch-cut description, which, in addition to being exact, leads to a useful physical picture of the relevant near- and intermediate-zone propagation physics for the considered problem. The method and model are described in Section II. Calculation results and analysis are provided in Section III, and we summarize our conclusions in Section IV.

II. Method and Simulation Model

The structure studied in this paper is a grounded multilayer medium, shown in Fig. 1(a). Fig. 1(b) depicts the chip structure of interest, with dimensions chosen to be the same as in [12]. A 633 $\mu\mathrm{m}$ thick grounded silicon wafer is covered by a 2 $\mu\mathrm{m}$ layer of silicon dioxide. The resistivity of silicon is taken to be 5 $\mathrm{k}\Omega-\mathrm{cm}$. In order to focus this study on basic propagation characteristics of the intra-chip channel, we use a Hertzian dipole radiator and determine the resulting electric field. Of course, the gain characteristics of a specific antenna will have an important influence on signal transmission and reception, and a variety of integrated antennas (zigzag, linear, meander, etc.) have been experimentally studied for intra-chip applications [3], [7], [8], [12]. Furthermore, since vertically polarized antennas only excite TM modes in a layered structure, whereas horizontally polarized antennas excite both TE and TM modes [13], to keep the propagation physics clear we assume a vertical Hertzian dipole. Nevertheless, for frequencies where only the TM_0 mode is above cutoff, we obtain similar results to previous experimental work on horizontal antennas, for reasons that are discussed later. Finally, the model assumes that the layered structure is laterally infinite and without any metal or other devices on it. A real IC chip obviously has finite dimensions, and metal lines or devices. Both the reflection and diffraction from the chip edges and those obstacles will certainly change signal propagation, and tend to depolarize the signal. However, these effects are beyond the scope of this paper. Moreover, since there is dielectric loss in at least the Si layer, the reflection and diffraction effects may play a small role for a suitably-large chip, although we don't attempt to estimate the required chip size so as to be able to ignore edge reflection and diffraction.

The Green functions and electric field relationships for the five-layer structure depicted in Fig. 1(a) are provided in the Appendix.

The vertical electric field due to a vertical Hertzian dipole when both the source and observation (field) points are in the same layer is

$$E_{xx}(\mathbf{r}) = \frac{1}{j\omega\varepsilon}\left(k^2+\frac{\partial^2}{\partial x^2}\right) \times \left(\frac{e^{-jk|\mathbf{r}-\mathbf{r}_s|}}{4\pi|\mathbf{r}-\mathbf{r}_s|}+\frac{-2\pi j}{2\pi}\sum_n \mathrm{Res}\left\{R_n(x,x',q_n)\right\}\right.$$

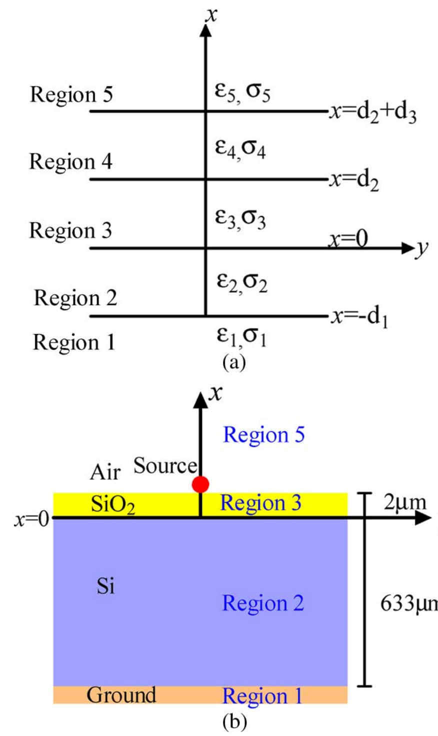

Fig. 1. (a) General multilayered dielectric medium. (b) Simple oxidized silicon substrate IC chip structure.

$$\left. \times \frac{H_0^{(2)}(q_n\rho)}{4p(q_n)}q_n + \frac{1}{2\pi}\int_{cb} R_n(x,x',q)\frac{H_0^{(2)}(q\rho)}{4p(q)}qdq\right) = E_{xx}^d(\mathbf{r}) + \sum_n E_{xx,n}^r(\mathbf{r}) + E_{xx}^{bc}(\mathbf{r}) \tag{1.1}$$

where all quantities are defined in the Appendix. The first term is the direct source-to-receiver (line of sight) contribution, the second term is a summation of residues associated with above cutoff TM surface waves ($\mathrm{q_n}$ is the nth surface wave propagation constant), and the last term is an integral over the hyperbolic branch cuts, representing the continuous spectrum, associated with a continuum of radiation modes of the structure. This decomposition of the field is exact.

It should be noted that the direct (line-of-sight) contribution can be incorporated into the continuous spectrum (see (1.6), which has no pole singularities). However, it is better to separate out this contribution, when possible, to clarify the propagation physics. To gain some understanding of the nature of the continuous spectrum in this representation, consider the case of no dielectric, so that we have a dipole source over a PEC plane. In this case, the total field is due to the direct (line-of sight) term and the radiation from an image dipole. In the spectral method, since there will be no residues/surface waves in this case (a single PEC plane cannot guide a surface wave, only a lossy conducting plane can), and since we have already separated-out the direct term, then the continuous spectrum must represent the image contribution. When one adds a dielectric the situation is more complicated, since if we write the total field as the direct contribution plus an "image" term, the latter is comprised of both surface waves and the continuous spectrum.

III. Results and Discussion

We first consider the four-layer structure consisting of a ground plane, silicon, silicon dioxide, and air layers, as shown in Fig. 1(b). For this case $d_3 = 0$, $\varepsilon_4 = \varepsilon_5 = \varepsilon_0$ and $\sigma_4 = \sigma_5 = 0$ in Fig. 1(a). In all cases the source is a vertical Hertzian dipole carrying a 20 mA current, and both source and observation points are in the top (air) layer. We assume $\varepsilon_{\mathrm{rSi}} = 11.9$ and $5\ \mathrm{k}\Omega - \mathrm{cm}$ resistivity, and $\varepsilon_{\mathrm{rSiO2}} = 4$.

A. Dispersion

The vertical electric field as a function of frequency is shown in Fig. 2 for a vertical Hertzian dipole source located in the air region at the air-$\mathrm{SiO_2}$ interface $(\mathrm{x} = 2\ \mu\mathrm{m})$. The source is located at $\rho = 0$, and the field is determined at the air-$\mathrm{SiO_2}$ interface at a lateral distance $\rho = 5\ \mathrm{mm}$, which was the source-receiver separation in several previous papers [3], [7], [8], [10], [12].

It can be seen that the branch cut and direct radiation contributions dominate over the residue (surface wave) contribution below 10 GHz. This is because at these frequencies the field position is electrically very close to the source. For example, at 10 GHz $\rho/\lambda_0 = 0.17$, where λ_0 is the wavelength in air. As frequency increases ρ/λ_0 becomes larger, and the residues may be expected to provide the dominant contribution to the total field. However, there are frequency spans where this is clearly not true. From 0 to 25 GHz, and from 45 to 90 GHz, the surface wave does not dominate the field, and both the branch cut and direct radiation are important. Furthermore, the dip at 71 GHz occurs due to destructive interference between the ground bounce wave and the direct field, caused by the condition $d = \lambda/2$, where d is the thickness of the Si substrate and λ is the wavelength in silicon.

The absence of a surface wave dominating the response in the 45 to 90 GHz range can be understood by considering the excitation amplitude of the surface wave, which is given by $\mathrm{Res}\{\mathrm{R_n(q_n)}\}$ in (1.1). Fig. 3(a) shows the absolute value of the fundamental mode surface wave excitation amplitude at the surface of a simple grounded dielectric slab having thickness $\mathrm{d} = 633\ \mu\mathrm{m}$, when the source is also at the slab surface. Different values of lossless permittivity $\varepsilon_\mathrm{r} = 2$, 10, 30, 60 are considered.

Note that this amplitude is independent of radial distance from the source. The dashed vertical lines show the condition $\mathrm{d} = \lambda/4$, where λ is the wavelength in the dielectric. Thus, the surface wave excitation amplitude peaks in the vicinity of the frequency where the corresponding slab thickness is a quarter wavelength in the dielectric. This can be interpreted as the wave traveling from the surface to the ground plane, and back to the surface, incurring a phase shift of 180 degrees. The additional 180 degree phase shift at the ground plane leads to a constructive interference, and a large excitation amplitude. The excitation amplitude peak is not exactly at the point $\mathrm{d} = \lambda/4$ since the dipole excites a spectrum of waves, and so we don't have simply a wave traveling vertically toward the ground plane.

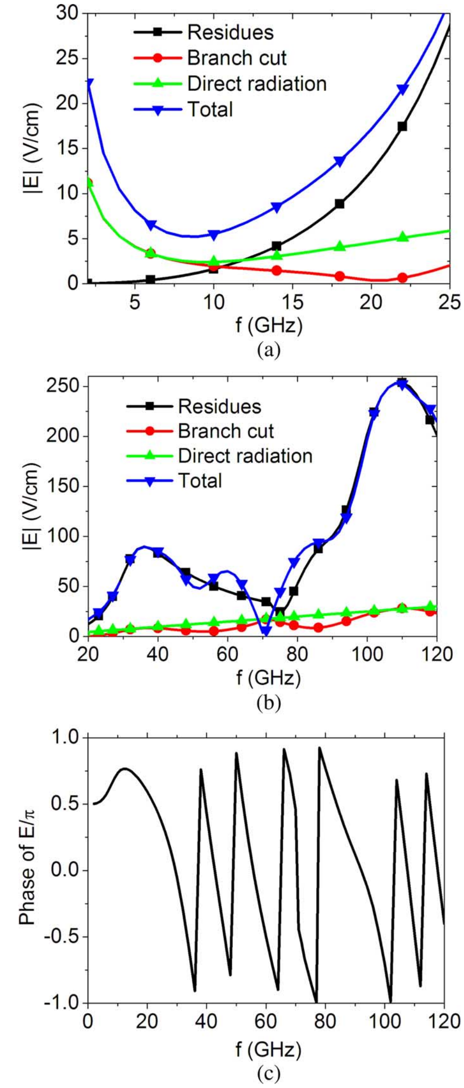

Fig. 2. (a) and (b) Magnitude of the electric field $\mathrm{E_{xx}}$ at the air-$\mathrm{SiO_2}$ interface $(\mathrm{x} = 2\ \mu\mathrm{m}, \rho = 5\ \mathrm{mm})$ for the structure shown in Fig. 1(b). Fig. 2(c) Phase of the total field (due to all wave components) for the same structure.

Fig. 3(b) shows the normalized surface wave propagation constant $\mathrm{q_n/k}$ for the TM fundamental mode $(\mathrm{n} = 0)$ of the grounded slab. It can be seen that the quarter wavelength condition corresponds to a region on the dispersion curve where the propagation constant is dramatically increasing (for large permittivity), such that the excitation amplitude peak is near the knee of the dispersion curve.

Therefore, in Fig. 2(b) the reason that the surface wave provides the dominant contribution near 35 GHz is because its excitation amplitude peaks there (in Fig. 3 the case $\varepsilon_\mathrm{r} = 10$ is close to silicon's value, and peaks at a slightly higher frequency than for silicon). The surface wave does not provide the dominant contribution in the 45 to 90 GHz range because its excitation amplitude falls off somewhat rapidly after 35 GHz, and the next mode does not start to propagate till approximately 72 GHz. Based on phase coherence, we would expect the next higher mode to have an excitation amplitude peak near where $\mathrm{d} = 3\lambda/4$, which would occur at approximately 103 GHz, which indeed corresponds to the second peak shown in Fig. 2(b).

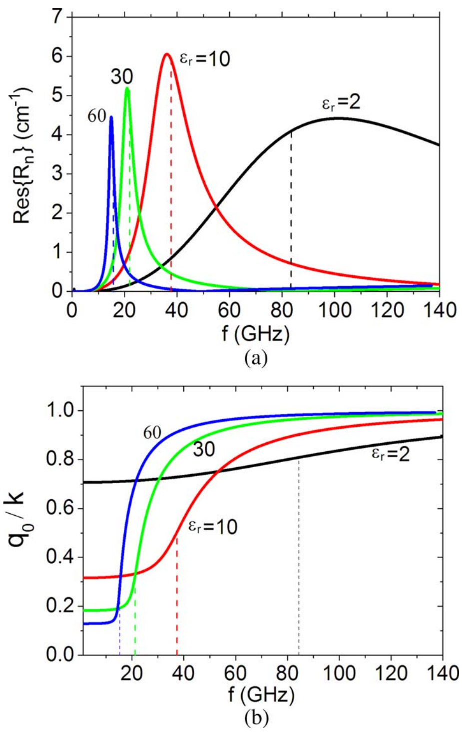

Fig. 3. (a) Absolute value of the fundamental mode surface wave excitation amplitude $\mathrm{Res}\{\mathrm{R_n}\}$ at the surface of a simple grounded dielectric slab having thickness $\mathrm{d} = 633\ \mu\mathrm{m}$ for different values of permittivity, $\varepsilon_\mathrm{r} = 2$, 10, 30, 60. The dashed vertical lines show the condition $\mathrm{d} = \lambda/4$, where λ is the wavelength in the dielectric. (b) Normalized surface wave propagation constant $\mathrm{q_n/k}$ (k is the wavenumber in the dielectric) for the TM fundamental mode $(\mathrm{n} = 0)$ of the grounded slab.

Therefore, the second surface wave dominates the response in the vicinity of its excitation peak, in the range 90 to 110 GHz (this second peak is not shown in Fig. 3, which only shows the excitation peaks for the fundamental mode).

Finally, it should be appreciated that, although the surface wave excitation amplitude is very important, it does not tell the entire story. For a lossless dielectric the surface wave decays as $1/\sqrt{\rho}$, and the direct term goes as $1/\rho$ (the continuous spectrum can have different behaviors depending on the structure, and may lead to lateral waves, etc.). Therefore, far from the source the surface wave may dominate even at frequencies quite different from its excitation amplitude peak. However, for lossy dielectrics as considered here, the role of the surface waves in the far field will be less important because of exponential attenuation of this component. For the near- and intermediate-field problem of interest in this work, the frequency dependence of the surface wave excitation amplitude perhaps plays the most important role in accessing the dominance of the surface wave.

The phase of the electric field is shown in Fig. 2(c). A constant linear phase profile is obviously desirable, otherwise signals will suffer distortion due to frequency dispersion. When multiple wave components contribute to the field, generally the phase will not have a constant linear profile, and, furthermore, deep nulls can occur due to destructive interference (e.g., near 71 GHz). It is seen that the phase is quite non-linear below 20 GHz. Multiple wave components (branch cut, residues, and direct radiation) lead to nonlinearities (for very small distances from the source these can be thought of as capacitive and inductive effects, rather than due to wave propagation). The phase changes linearly between approximately 30 and 55 GHz, the range surrounding the surface wave excitation peak (as seen in Fig. 3(a), the peak is asymmetric, falling off more slowly on the high-frequency side), but then becomes nonlinear. The same highly nonlinear phase profile in the 60–70 GHz range was found in the measured transmission phase in [12], even though in that work horizontal polarization was used. Linearity is somewhat restored after 80 GHz, but the slope changes after approximately 90 GHz. The worst phase behavior is from 55 to 90 GHz, which, from Fig. 2(b), is the frequency span where multiple wave components contribute strongly to the field (this will be discussed further in the next section). The same phenomenon is also mentioned in [7] and [12]. This shows the importance of achieving a mono-component propagation channel for signal integrity.

Multipath typically refers to a ray model, where the field contributions come from signals that take different physical routes to the receiver. For the near- and intermediate-field problem of interest here, this concept needs to be generalized, since a ray model is not as appropriate. In this case, there are actual multipath effects, such as interference between the direct source-to-receiver radiation and the surface guided energy (which implicitly includes ground bounce terms), but there are also interference effects due to multiple spectral (e.g., discrete and continuous) components, leading to what we will call a *generalized multipath* problem.

Parenthetically, it is worthwhile to note that, rather than decomposing the spectral integral (1.8) as a sum of residues and a branch cut, one may rewrite the spectral coefficients as a ray series. For example, for a simple grounded dielectric characterized by ε_2 and thickness d, covered by a dielectric characterized by ε_1, the spectral coefficient analogous to (1.9) is

$$\begin{aligned} R_n &= \frac{n_{21}^2 p_1 - p_2 \tanh(p_2 d)}{n_{21}^2 p_1 + p_2 \tanh(p_2 d)} = \frac{-K + e^{-2p_2 d}}{1 - K e^{-2p_2 d}} \\ &= -K + (1 - K^2) e^{-2p_2 d} + K(1 - K^2) e^{-4p_2 d} \\ &\quad + K^2 e^{-6p_2 d} + \cdots \end{aligned} \tag{1.2}$$

where $n_{21}^2 = \varepsilon_2/\varepsilon_1$, $p_{1,2}$ are defined in the Appendix, and

$$K = \frac{p_2 - n_{21}^2 p_1}{p_2 + n_{21}^2 p_1}. \tag{1.3}$$

The series form is obtained using the geometric series

$$\frac{1}{1-r} = \sum_{n=0}^{\infty} r^n \tag{1.4}$$

with $r = K e^{-2p_2 d}$. For field positions sufficiently far from the source, the resulting spectral integrals can be approximated using, e.g., the method of steepest descents, in which case it would be seen that the first term represents the reflection from the interface, the second term represents the wave that is transmitted into the substrate, reflects off of the ground plane, and then comes back out into the air region, and the subsequent terms represent an increasing number of "bounces" inside the substrate. The resulting ray decomposition is also exact,

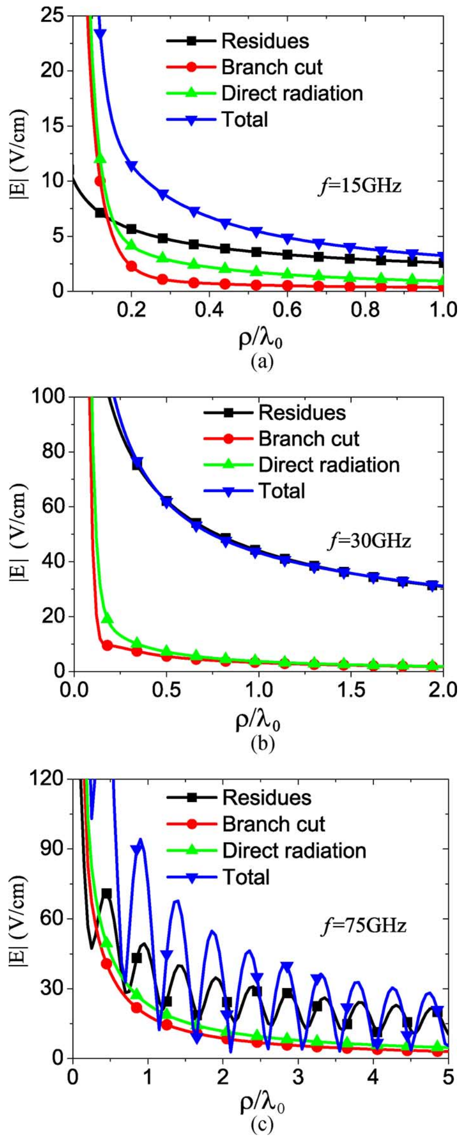

Fig. 4. Magnitude of the electric field E_{xx} at the air-SiO_2 interface ($x = 2\ \mu m$) for the structure shown in Fig. 1(b).

although the spectral decomposition makes more sense for the near- and intermediate-field problem considered here.

B. Relationship of Dominant Wave Component and Horizontal Distance From the Source

In order to further investigate the behavior of the various wave components, Fig. 4 shows the magnitude of the vertical electric field at three different frequencies, as horizontal distance changes.

We assume that the source point and observation point are both on the surface of the oxidized silicon ($x = 2\ \mu m$), and we let ρ vary. At 15 GHz, $\lambda_0 = 20$ mm, and so if we take $\rho_{max} = 20$ mm as a typical maximal chip dimension of interest, then we are interested in the range $0 < \rho/\lambda_0 < 1$. For 30 GHz, the range of interest is $0 < \rho/\lambda_0 < 2$, and for 75 GHz, since $\lambda_0 = 4$ mm, we are interested in the approximate range $0 < \rho/\lambda_0 < 5$. At 15 and 30 GHz, only the TM_0 mode is above cutoff. At 75 GHz, two TM surface waves are above cutoff, TM_0 and TM_2, although the TM_2 mode is dominant over the TM_0 mode.

It can be seen from Fig. 4 that for the 15 GHz case, in the range $0 < \rho/\lambda_0 < 1$, no single wave component approximates the total field. For $\rho/\lambda_0 > 1$ the surface wave becomes dominant, but these lateral distances are typically not of interest for intra-chip communications.

At 30 GHz, the surface wave dominates the field for essentially all lateral distances of interest. For 75 GHz in the range of interest $0 < \rho/\lambda_0 < 5$, no single wave component dominants the total field. Although this frequency is near a dip in the frequency dispersion curve, as can be seen from Fig. 2(b), the same comments about lack of a dominant surface wave would apply for most frequencies in the range $0 < f < 25$ GHz and 45 GHz $< f < 90$ GHz. Likewise, the dominance of the surface wave field, as in Fig. 4(b) at 30 GHz, will be found typically in the range 25 GHz $< f < 45$ GHz, and 90 GHz $< f < 110$ GHz. Thus, although surface wave contributions are generally quite strong in layered media, given the small chip dimensions of practical interest, the problem is essentially a near- and intermediate-field problem, and often no single wave component dominates the response.

Previous measurement on this chip structure have shown that the path loss exponent is approximately 1.4, much smaller than 2 (the PLE in air), pointing to the surface wave as an important field constituent [12]. The findings in this work are complementary to those measurements, but point to a more complicated interplay among various wave components. As frequency varies, the distance at which the surface wave begins to dominate the total field varies. There are many frequency spans where, assuming a maximum practical chip size of 20 mm, the surface wave never dominates the total field (e.g., see Fig. 4(a) and (c)). At other frequencies, in the span 25 to 45 GHz, and 90 to 110 GHz, the surface wave tends to dominate the field for relatively small source-receiver separations [see, e.g., Fig. 4(b)], due to the location of the surface wave excitation amplitude peak. Therefore, for a given chip structure the frequency span for mono-component wave propagation needs to be carefully determined. The design of an intra-chip communication system must account for these generalized multipath effects.

C. Relationship Between Dominant Wave Component and Vertical Distance From the Source

The variation of the electric field with height above the SiO_2 at lateral distances $\rho/\lambda_0 = 0.1$ and 1.0 is shown in Fig. 5.

When $\rho/\lambda_0 = 0.1$ and x/λ_0 is small, all of the wave components (discrete and continuous spectrum, and direct radiation) contribute significantly to the total field. As x/λ_0 increases, the branch cut and surface wave contributions become equal and opposite, and tend to cancel each other out, such that the direct radiation term is dominant; however, the total field is very small. For the value $\rho/\lambda_0 = 1.0$, when x increases, the branch cut and direct radiation will contribute more than the residues, as shown Fig. 5(c). Both Fig. 4 and Fig. 5 indicate that the dominant wave component depends on the electrical thickness of the substrate, and on the distances ρ/λ_0 and x/λ_0.

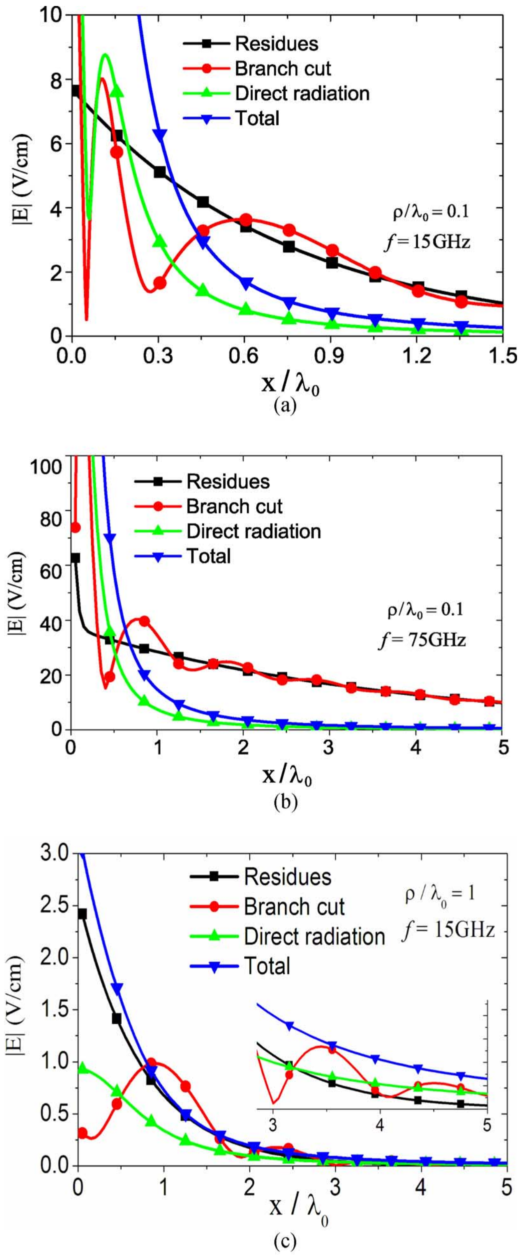

Fig. 5. Magnitude of the electric field E_{xx} for two different frequencies, as a function of height above the SiO_2 for the structure shown in Fig. 1(b).

D. Propagation Improvement by Using Guiding Layers

Given the basic IC chip structure depicted in Fig. 1(b), a natural question arises as to if improvements in the structure can be made that favor certain types of wave propagation. It seems that a natural candidate for transmission enhancement is the surface wave, since at many frequencies this is the strongest wave component, and perhaps the easiest to control. Enhancement of surface waves is exactly the opposite of what is desired for typical microstrip antenna applications, where minimization or elimination of surface waves is the objective [28]. A popular method to suppress surface waves and achieve a resonant gain structure is by using a dielectric superstrate over the antenna [25]–[27]. Here we consider adding either a dielectric superstrate or an additional substrate to enhance surface wave propagation at a certain frequency, and numerically determine the optimum layer thickness for a given material. This was also done experimentally in [9], [10], where a "guiding layer" was inserted between the silicon wafer and ground plane to improve the gain of the integrated antennas. In this section the effect of different guiding layers on the electric field is discussed. In general, the addition of a guiding layer will enhance surface wave propagation, since, as the total thickness of the dielectric structure is increased, more energy from a source tends to be carried by surface waves. It must also be kept in mind that increasing the surface wave component will tend to increase crosstalk (the intra-chip channel is really a form of intentional mutual coupling between two integrated antennas). Ideally, the intra-chip antennas should more strongly excite surface waves than on-chip devices. More to the point, on-chip devices should excite surface waves to a sufficiently low degree that unintentional cross-talk is manageable (intra-chip antennas should effectively utilize the on-chip propagation channel, whereas on-chip devices should not couple strongly to this channel). Strategies for eliminating surface wave excitation, such as considered in [28], may be useful in this regard.

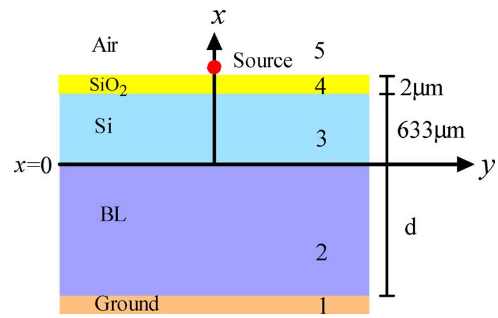

Fig. 6. Chip geometry including a bottom layer for enhanced waveguiding.

We will consider the 15 GHz case, which was considered in previous experimental work, and where, from Fig. 2(a), it can be seen that all three wave components are important for the original (unenhanced) structure.

1) Bottom Guiding Layer: We first consider a guiding layer between the silicon and the ground plane [designated as a bottom layer (BL)], and determine the electric field at 15 GHz for the case of both transmitting dipole and observation point located on the surface of the SiO_2, as depicted in Fig. 6.

Two different kinds of material are chosen as the bottom layer: glass, with $\varepsilon_r = 5.5$ and $\sigma = 0$, and aluminum nitride (AlN), with $\varepsilon_r = 8.5$ and $tan\delta = 0.008$. The permittivity of several AlN materials fabricated by different companies was measured in [29], and the average value was chosen for our calculation. The electric field for the geometry that includes the bottom layer, normalized by the field for the case of no bottom layer, is shown in Fig. 7 and Fig. 8.

Fig. 7(a) shows the surface wave component of the electric field with glass as a bottom guiding layer, normalized by the field without the glass layer, for different values of the bottom layer thickness. It can be seen that $d = 0.85$ mm provides the largest enhancement of the residue field. This value of glass thickness also provides the largest enhancement of the total field, as seen in Fig. 7(b). From Fig. 7(c), it can be seen that

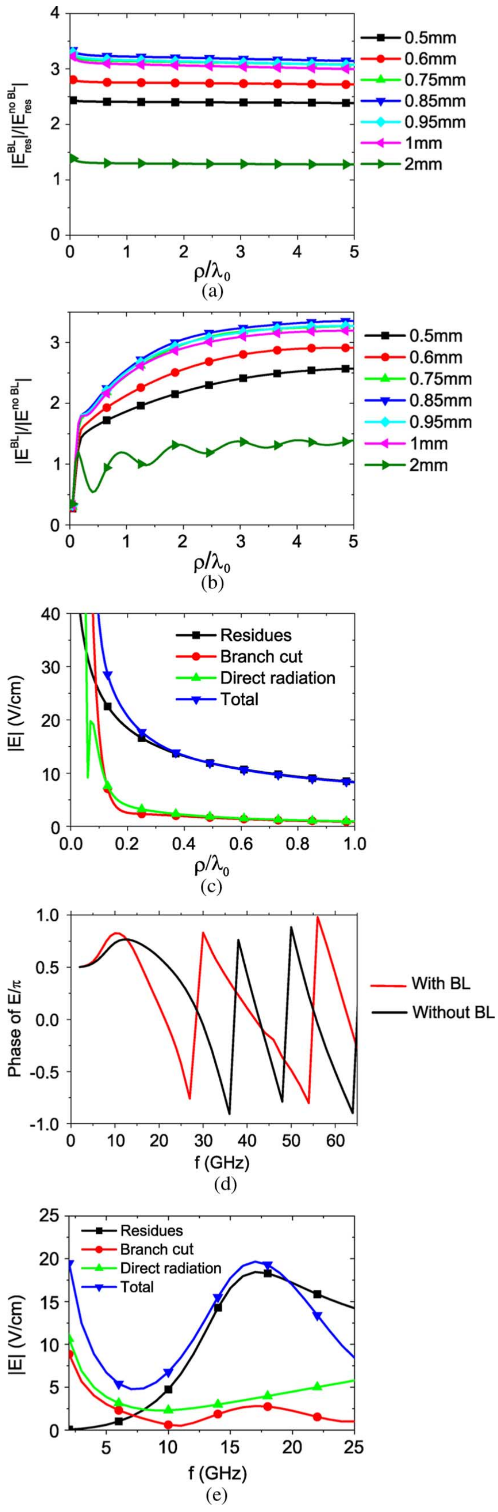

Fig. 7. (a). Comparison between the residue component of the electric field with glass as a bottom guiding layer (E_{res}^{BL}) normalized by the same field component without the glass layer $(E_{res}^{no\ BL})$, for different values of the bottom layer thickness; (b) shows the same thing as (a), except for the total field. (c) Non-normalized field components for $d = 0.85$ mm as the lateral source-receiver separation varies. (d) Comparison between the phase of the total field with a 0.85 mm glass BL and without a BL, for $\rho = 5$ mm. (e) Magnitude of the electric field E_{xx} at the air-SiO_2 interface for the structure shown in Fig. 6 with a $d = 0.85$ mm glass BL, $\rho = 5$ mm.

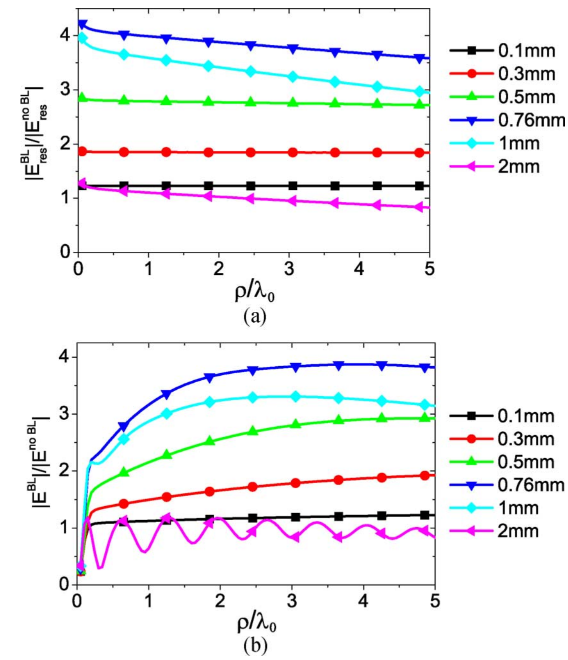

Fig. 8. (a). Comparison between the residue component of the electric field with AlN as a bottom guiding layer (E_{res}^{BL}) normalized by the same field component without the AlN layer $(E_{res}^{no\ BL})$, for different values of the bottom layer thickness; (b) shows the same thing as (a), except for the total field.

the enhancement of the total field is mainly due to the residue enhancement, since the total field is dominated by the residue contribution starting at a relatively small value of lateral separation, $\rho/\lambda_0 = 0.3$ (compare with Fig. 4(a), where $\rho/\lambda_0 > 1$ for the residue component to dominate the total field). This means that the structure with a glass bottom layer having the correct value of thickness can preferentially enhance the surface wave at a given frequency, and lead to the reduction of generalized multipath effects.

Fig. 7(d) shows that phase linearity is indeed improved at 15 GHz due to the addition of the bottom layer. However, as can be seen from Fig. 7(e), this improvement holds near 15 GHz, and at other frequencies a different value of bottom layer thickness would be needed to optimize performance.

For the AlN bottom layer, the field can also be enhanced by proper choice of the layer thickness as shown in Fig. 8. The optimal thickness of the AlN layer that provides the largest enhancement of the surface wave and total field is 0.76 mm. In [10], an improvement of 8 dB was measured using a 0.76 mm AlN bottom layer, for a horizontally polarized antenna (which will excite both TE and TM surface waves). From Fig. 8(b), we compute a total field increase of approximately 7.04 dB for vertical polarization.

Despite the polarization difference, this general agreement makes sense because for this structure, at 15 GHz, only the TM_0 mode propagates (all TE modes are below cutoff), and so for an antenna having either polarization, surface wave energy is carried by the TM_0 mode.

Finally, it should be noted that the cutoff frequency of the second surface wave mode is 39 GHz for the glass guiding layer, under conditions of optimal thickness 0.85 mm, and 37 GHz for the AlN layer, for optimal thickness 0.76 mm. These cutoff frequencies are obviously lower than the value for the original structure (72 GHz), due to the increase of the total dielectric thickness. These frequencies represent the limits for single mode propagation.

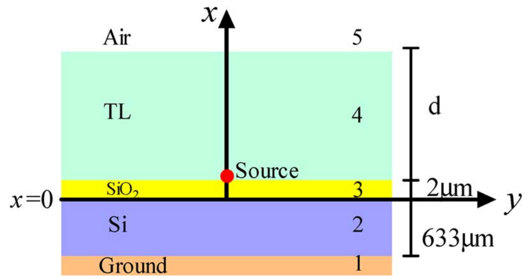

Fig. 9. IC structure with a waveguiding top layer (TL).

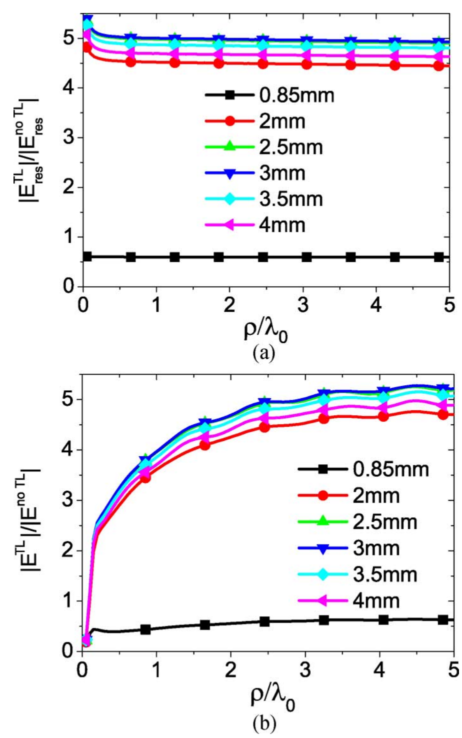

Fig. 10. (a). Comparison between the residue component of the electric field with glass as a top guiding layer (E_{res}^{TL}) normalized by the same field component without the glass layer ($E_{res}^{no\ TL}$), for different values of the top layer thickness. (b) shows the same thing as (a), except for the total field.

2) Top Guiding Layer: In this section we consider a guiding layer on top of the silicon dioxide [designated as a top layer (TL)], as depicted in Fig. 9. The source dipole and field observation point are both located on top of the silicon dioxide layer, as before, and the fields are determined at 15 GHz.

Glass and AlN are again chosen as the guiding layer material. The electric field on top of the SiO_2 layer, normalized by the field in a structure without a top layer, is shown in Fig. 10 for glass and Fig. 11 for AlN.

When the glass is put on top of a silicon substrate, both the electric field due to surface waves, and the total field are increased. The optimal thickness corresponding to the largest enhancement is 3 mm for both the surface wave component and the total field. This implies that a top guiding layer with correctly chosen thickness can enhance the surface wave at a given frequency. Note that the enhancement for the top guiding layer is larger than that for the case of a bottom guiding layer, although the top layer thickness is also much larger than the bottom layer

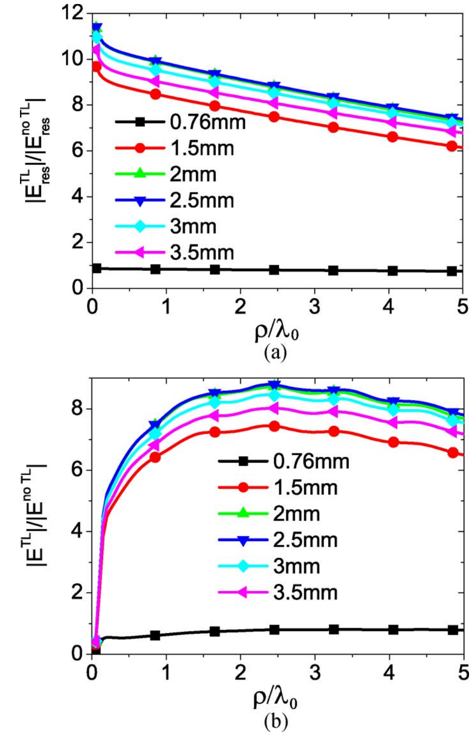

Fig. 11. Same as Fig. 10, except for AlN as the top guiding layer.

thickness. This is because the vertical surface wave field of the dominant mode is maximum at the ground plane, and decreases towards the air interface. Consequently, when the source is at the top of the dielectric layer (in the case of an added bottom guiding layer), the surface wave excitation is less than when the source is near the middle of the dielectric layers (which occurs in the case of an added top guiding layer).

For AlN as the top guiding layer, the enhancement is almost twice as much as that for a glass top guiding layer at lateral distances smaller than λ_0. The optimal thickness corresponding to the largest enhancement is 2.5 mm in this case, much thicker than 0.76 mm when AlN is used as a bottom guiding layer. The field attenuates with increasing lateral separation because of dielectric loss in the AlN layer. The cutoff frequency of the second surface wave mode is decreased to 20 GHz for 3 mm glass, and 17 GHz for 2.5 mm AlN, due to the addition of the much thicker top guiding layer, defining the range for single mode propagation.

IV. Conclusion

Fundamental wave propagation mechanisms for intra-chip communications in a multilayered IC chip structure have been studied by determining the electric field due to a Hertzian dipole source. An examination of the electric field as a function of frequency for practical source-receiver separations shows that the surface wave may or may not provide the dominant propagation channel, even on the substrate surface. Given the small dimensions of a typical IC chip, at most frequencies of interest we need to consider the near- and intermediate-field problem, where continuous spectral components (branch cut) and direct radiation play important roles in propagation. This leads to a generalization of the concept of the ray-model of multipath, to include multiple spectral (e.g., discrete and continuous) components. The surface wave excitation amplitude is an important factor in determining if the surface wave will dominate the field at a given frequency.

The effect of a guiding layer placed either below or above the silicon substrate has also been discussed. Both types of layers can enhance fields. An optimal thickness of the guiding layer can be found that preferentially enhances surface wave propagation. The occurrence of such a mono-component propagation channel is desirable from a dispersion standpoint, and to avoid interference nulls due to multipath. For the short transmission distances encountered on an IC chip, both glass and AlN guiding layers lead to enhanced waveguiding.

APPENDIX

The electric field in region α due to a current in region β of a multilayered medium as depicted in Fig. 1(a) is [30], [31]

$$\mathbf{E}^{\alpha}(\mathbf{r}) = \left(k_{\alpha}^{2} + \nabla\nabla\cdot\right) \int_{\Omega} \left\{\delta_{\alpha\beta}\underline{\mathbf{g}}^{p}(\mathbf{r},\mathbf{r}') + \underline{\mathbf{g}}^{s}(\mathbf{r},\mathbf{r}')\right\} \cdot \frac{\mathbf{J}(\mathbf{r}')}{j\omega\varepsilon_{\beta}} d\mathbf{r}' \tag{1.5}$$

where $\delta_{\alpha\beta}$ is the Kronecker delta function

$$\begin{aligned}\underline{\mathbf{g}}^{p}(\mathbf{r},\mathbf{r}') &= \underline{\mathbf{I}}\frac{e^{-jk_{\beta}|\mathbf{r}-\mathbf{r}'|}}{4\pi|\mathbf{r}-\mathbf{r}'|} \\ &= \underline{\mathbf{I}}\frac{1}{2\pi}\int_{-\infty}^{\infty} e^{-p_{\beta}|x-x'|}\frac{H_0^{(2)}(q\rho)}{4p_{\beta}(q)} q\,dq \end{aligned} \tag{1.6}$$

with $p_i^2 = q^2 - k_i^2$, $q^2 = k_y^2 + k_z^2$ (q is a radial wavenumber), and $k_i = \omega\sqrt{\mu_i\varepsilon_i}$. For convergence of the integral, and to ensure the proper field behavior at infinity, we require $\mathrm{Re}\{p_{\mathrm{j}}\} > 0$ in the outermost region (the region in which $x \to \infty$), which determines hyperbolic branch cuts in the complex q-plane [14]. Also

$$\underline{\mathbf{g}}^{s}(\mathbf{r},\mathbf{r}') = \hat{\mathbf{x}}\hat{\mathbf{x}}g_n^s(\mathbf{r},\mathbf{r}') + \left(\hat{\mathbf{x}}\hat{\mathbf{y}}\frac{\partial}{\partial y} + \hat{\mathbf{x}}\hat{\mathbf{z}}\frac{\partial}{\partial z}\right) g_c^s(\mathbf{r},\mathbf{r}') + (\hat{\mathbf{y}}\hat{\mathbf{y}} + \hat{\mathbf{z}}\hat{\mathbf{z}})g_t^s(\mathbf{r},\mathbf{r}') \tag{1.7}$$

where

$$\left.\begin{matrix} g_t^s(\mathbf{r},\mathbf{r}') \\ g_n^s(\mathbf{r},\mathbf{r}') \\ g_c^s(\mathbf{r},\mathbf{r}') \end{matrix}\right\} = \frac{1}{2\pi}\int_{-\infty}^{\infty} \left\{\begin{matrix} R_t(x,x',q) \\ R_n(x,x',q) \\ R_c(x,x',q) \end{matrix}\right\} \frac{H_0^{(2)}(q\rho)}{4p_{\beta}(q)} q\,dq \tag{1.8}$$

and $\rho = \sqrt{(y-y')^2 + (z-z')^2}$. The coefficients $R_j(x,x',q)$ are determined by the specific structure of the layered medium. The Hankel function represents radial propagation, since, for $q\rho \gg 1$

$$H_0^{(2)}(q\rho) \simeq \sqrt{\frac{2}{\pi q\rho}} e^{-j(q\rho - \pi/4)}.$$

The expression for the vertical field in the same layer as a vertical Hertzian dipole $\mathbf{J}(\mathbf{r}) = \hat{x}\delta(\mathbf{r} - \mathbf{r}_s)$ is (1.1), obtained via complex plane analysis (see, e.g., [14, Ch. 5,] or [15, Ch. 11]).

For the five-layer structure depicted in Fig. 1(a), when the source and observation points are in the top region, the coefficient R_n is

$$R_n(x,x',q) = \frac{N^E(q)}{Z^E(q)} e^{-p_5(x+x')} \tag{1.9}$$

where

$$\begin{aligned} N^E &= p_5\varepsilon_4\left[C_{o3}e^{p_4(d_2+d_3)} + e^{-p_4(d_2+d_3)}\right] \\ &\quad - p_4\varepsilon_5\left[C_{o3}e^{p_4(d_2+d_3)} - e^{-p_4(d_2+d_3)}\right] \end{aligned} \tag{1.10}$$

$$\begin{aligned} Z^E &= p_5\varepsilon_4\left[C_{o3}e^{p_4(d_2+d_3)} + e^{-p_4(d_2+d_3)}\right] \\ &\quad + p_4\varepsilon_5\left[C_{o3}e^{p_4(d_2+d_3)} - e^{-p_4(d_2+d_3)}\right] \end{aligned} \tag{1.11}$$

$$C_{03} = e^{-2p_4d_2}\frac{1+M_{o3}}{1-M_{o3}} \tag{1.12}$$

and M_{o3} is given in (1.13) at the bottom of page. Other coefficients are obtained for other source-observation point locations.

The terms involving R_t are associated with TE modes, those involving R_n are associated with TM modes, and the terms associated with R_c have both TE and TM mode contributions. Since the residue and branch cut contributions associated with a horizontal source are more complicated due to the excitation of both TE and TM modes, here we have restricted attention to the field E_{xx}. However, for completeness we mention that the horizontal field in the same layer as a horizontal Hertzian dipole $\mathbf{J}(\mathbf{r}) = \hat{\mathbf{y}}\delta(\mathbf{r} - \mathbf{r}_s)$ is (1.14)

$$\begin{aligned} E_{yy}(\mathbf{r}) =& \frac{1}{j\omega\varepsilon}\left(k^2 + \frac{\partial^2}{\partial y^2}\right) \\ &\times \left(\frac{e^{-jk|\mathbf{r}-\mathbf{r}_s|}}{4\pi|\mathbf{r}-\mathbf{r}_s|} + \frac{-2\pi j}{2\pi}\sum_n \mathrm{pRes}\left\{R_n(x,x',q_n)\right\}\right. \\ &\times \frac{H_0^{(2)}(q_n\rho)}{4p(q_n)} q_n + \frac{1}{2\pi} \\ &\times \left.\int_{cb} R_n(x,x',q)\frac{H_0^{(2)}(q_n\rho)}{4p(q_n)} q_n\,dq\right) + \frac{1}{j\omega\varepsilon} \\ &\times \frac{\partial^3}{\partial x\partial y^2}\left(\frac{-2\pi j}{2\pi}\sum_n \mathrm{Res}\left\{R_c(x,x',q_n)\right\}\right. \\ &\times \frac{H_0^{(2)}(q_n\rho)}{4p(q_n)} q_n + \frac{1}{2\pi} \\ &\times \left.\int_{cb} R_c(x,x',q)\frac{H_0^{(2)}(q\rho)}{4p(q)} q\,dq\right). \end{aligned} \tag{1.14}$$

$$M_{o3} = \frac{p_3\varepsilon_4}{p_4\varepsilon_3}\frac{\sinh(p_3d_2)p_3\varepsilon_2\left[p_2\varepsilon_1\cosh(p_2d_1) + p_1\varepsilon_2\sinh(p_2d_1)\right] + \cosh(p_3d_2)p_2\varepsilon_3\left[p_2\varepsilon_1\sinh(p_2d_1) + p_1\varepsilon_2\cosh(p_2d_1)\right]}{\cosh(p_3d_2)p_3\varepsilon_2\left[p_2\varepsilon_1\cosh(p_2d_1) + p_1\varepsilon_2\sinh(p_2d_1)\right] + \sinh(p_3d_2)p_2\varepsilon_3\left[p_2\varepsilon_1\sinh(p_2d_1) + p_1\varepsilon_2\cosh(p_2d_1)\right]} \tag{1.13}$$

REFERENCES

[1] Z. M. Chen and Y. P. Zhang, "Inter-chip wireless communication channel: Measurement, characterization, and modeling," *IEEE Trans. Antennas Propag.*, vol. 55, no. 3, pp. 978–986, Mar. 2007.

[2] M. F. Chang, V. P. Roychowdhury, L. Zhang, H. Shin, and Y. X. Qian, "RF/wireless interconnect for Inter- and Intra-chip communications," *Proc. IEEE*, vol. 89, no. 4, pp. 456–466, Apr. 2001.

[3] B. A. Floyd, C.-M. Hung, and K. K. O, "Intra-chip wireless interconnect for clock distribution implemented with integrated antennas, receivers, and transmitters," *IEEE J. Solid-State Circuits*, vol. 37, no. 5, pp. 543–552, May 2002.

[4] Y. J. Zheng, Y. P. Zhang, and Y. Tong, "A novel wireless interconnect technology using impulse radio for interchip communications," *IEEE Trans. Microw. Theory Tech.*, vol. 54, no. 4, pp. 1912–1920, Apr. 2006.

[5] M. Sun and Y. P. Zhang, "Performance of inter-chip RF-interconnect using CPW, capacitive coupler, and UWB transceiver," *IEEE Trans. Microw. Theory Tech.*, vol. 53, no. 9, pp. 2650–2655, Sept. 2005.

[6] Y. P. Zhang, L. H. Guo, and M. Sun, "High transmission gain inverted-F antenna on low resistivity Si for wireless interconnect," *IEEE Electron Device Lett.*, vol. 27, no. 5, pp. 374–376, May 2006.

[7] Y. P. Zhang, M. Sun, and W. Fan, "Performance of integrated antennas on silicon substrates of high and low resistivities up to 110 GHz for wireless interconnects," *Microw. Opt. Technol. Lett.*, vol. 48, no. 2, pp. 302–305, Feb. 2006.

[8] K. Kim and K. K. O, "Characteristics of integrated dipole antennas on Bulk, SOI, and SOS substrates for wireless communication," in *Proc IITC*, San Francisco, 1998, pp. 21–23.

[9] K. Kim, W. Bomstad, and K. K. O, "A plane wave model approach to understanding propagation in an intra-chip communication system," in *Proc. IEEE Int. Symp. AP-S*, Boston, MA, 2001, vol. 2, pp. 166–169.

[10] X. L. Guo, J. Caserta, R. Li, B. Floyd, and K. K. O., "Propagation layers for intra-chip wireless interconnection compatible with packaging and heat removal," in *Proc. VLSI Technol. Symp.*, 2002, pp. 36–37.

[11] T. Kikkawa, A. B. M. H. Rashid, and S. Watanabe, "Effect of silicon substrate on the transmission characteristics of integrated antenna," in *IEEE Topical Conf. on Wireless Commun. Technol.*, 2003, pp. 144–145.

[12] Y. P. Zhang, Z. M. Chen, and M. Sun, "Propagation mechanisms of radio waves over intra-chip channels with integrated antennas: Frequency-domain measurements and time-domain analysis," *IEEE Trans. Antennas Propag.*, vol. 55, no. 10, pp. 2900–2906, Oct. 2007.

[13] J. R. Wait, *Electromagnetic Waves in Stratified Media*. New York: Pergamon Press, 1962.

[14] L. B. Felsen and N. Marcuvitz, *Radiation and Scattering of Waves*. New York: IEEE Press, 1994.

[15] R. E. Collin, *Field Theory of Guided Waves*, 2nd ed. New York: IEEE Press, 1991.

[16] D. Marcuse, *Theory of Dielectric Optical Waveguides*. New York: Academic Press, 1974.

[17] V. Shevchenko, *Continuous Transitions in Open Waveguides*. Boulder, CO: Golem Press, 1971.

[18] J. R. Mosig and F. E. Gardiol, "Analytical and numerical techniques in the Green's function treatment of microstrip antennas and scatterers," *IEE Proc.*, vol. 130, no. 2, pt. H, Mar. 1983.

[19] Y. L. Chow, J. J. Yang, D. G. Fang, and G. E. Howard, "A closed-form spatial Green's function for the thick microstrip substrate," *IEEE Trans. Microw. Theory Tech.*, vol. 39, no. 3, Mar. 1991.

[20] M. A. Marin and P. H. Pathak, "An asymptotic closed-form representation for the grounded double-layer surface Green's function," *IEEE Trans. Antennas Propag.*, vol. 41, no. 11, Nov. 1992.

[21] M. I. Aksun and R. Mittra, "Derivation of closed-form Green's functions for a general microstrip geometry," *IEEE Trans. Microw. Theory Tech.*, vol. 40, no. 11, Nov. 1992.

[22] F. J. Demuynck, G. A. E. Vandenbosch, and A. R. Van de Capelle, "The expansion wave concept-Part I: Efficient calculation of spatial Green's functions in a stratified dielectric medium," *IEEE Trans. Antennas Propag.*, vol. 46, no. 3, Mar. 1998.

[23] M. I. Aksun and G. Dural, "Clarification of issues on the closed-form Green's functions in stratified media," *IEEE Trans. Antennas Propag.*, vol. 53, no. 11, Nov. 2005.

[24] F. Mesa, R. R. Boix, and F. Medina, "Closed-form expressions of multilayered planar Green's functions that account for the continuous spectrum in the far field," *IEEE Trans. Microw. Theory Tech.*, vol. 56, no. 7, July 2008.

[25] D. Jackson and N. G. Alexópoulos, "Fundamental superstrate (cover) effects on printed circuit antennas," *IEEE Trans. Antennas Propag.*, vol. AP-32, no. 8, Aug. 1984.

[26] N. G. Alexópoulos and D. Jackson, "Gain enhancement methods for printed circuit antennas," *IEEE Trans. Antennas Propag.*, vol. AP-33, no. 9, Sept. 1985.

[27] Y. Sugio, T. Makimoto, S. Nishimura, and H. Nakanishi, "Analysis for gain enhancement of multiple-relection line antenna with with dielectric plates," *Trans. IECE*, pp. 80–112, Jan. 1981.

[28] D. R. Jackson, J. T. Williams, A. K. Bhattacharyya, R. L. Smith, S. J. Buchheit, and S. A. Long, "Microstrip patch designs that do not excite surface waves," *IEEE Trans. Antennas Propag.*, vol. 41, no. 8, Aug. 1993.

[29] P. Wright and L. E. Davis, "The complex permittivity of aluminum nitride substrates," in *IEEE MTT-S Digest*, 1993, pp. 269–272.

[30] J. S. Bagby and D. P. Nyquist, "Dyadic Green's functions for integrated electronic and optical circuits," *IEEE Trans. Microw. Theory Tech.*, vol. MTT-35, pp. 206–210, Feb. 1987.

[31] G. W. Hanson and A. B. Yakovlev, *Operator Theory for Electromagnetics*. New York: Springer, 2002.

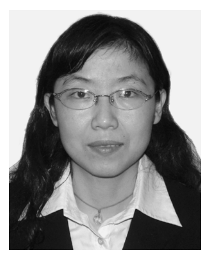

Liping Yan (M'08) was born in Hebei, China, in 1972. She received the B.S. degree from Hebei Normal University, Shijiazhuang, China in 1993, and the M.S. and Ph.D. degrees from Sichuan University, Chengdu, China, in 1996 and 2003, respectively.

From March 2008 to March 2009, she was a Visiting Scholar at the Department of Electrical Engineering and Computer Science, University of Wisconsin in Milwaukee, where she worked on wave propagation mechanisms in multilayer structures frequently used for intra-chip wireless communications. She is currently Associate Professor in the College of Electronics and Information Engineering, Sichuan University. Her research interests include numerical simulation in electromagnetics, electromagnetic wave phenomena in layered media, design of applicators and probes for biomedical applications, and antennas.

Dr. Yan is a Senior Member of the Chinese Institute of Electronics.

George W. Hanson (M'91–SM'98–F'08) was born in Glen Ridge, NJ, in 1963. He received the B.S.E.E. degree from Lehigh University, Bethlehem, PA, the M.S.E.E. degree from Southern Methodist University, Dallas, TX, and the Ph.D. degree from Michigan State University, East Lansing, in 1986, 1988, and 1991, respectively.

From 1986 to 1988, he was a Development Engineer with General Dynamics in Fort Worth, TX, where he worked on radar simulators. From 1988 to 1991, he was a Research and Teaching Assistant in the Department of Electrical Engineering, Michigan State University. He is currently a Professor of electrical engineering and computer science, University of Wisconsin in Milwaukee. His research interests include nanoelectromagnetics, mathematical methods in electromagnetics, electromagnetic wave phenomena in layered media, integrated transmission lines, waveguides, and antennas, and leaky wave phenomena.

Dr. Hanson is a member of URSI Commission B, Sigma Xi, and Eta Kappa Nu, and was an Associate Editor for the IEEE TRANSACTIONS ON ANTENNAS AND PROPAGATION from 2002–2007. In 2006 he received the S.A. Schelkunoff Best Paper Award from the IEEE Antennas and Propagation Society.